SICE Annual Conference 2008
August 20-22, 2008, The University Electro-Communications, Japan

3D Shape Measuring Sheet Utilizing Gravitational and Geomagnetic Fields

Takayuki Hoshi[1] and Hiroyuki Shinoda[1]

[1]Department of Information Physics and Computing, Graduate School of Information Science and Technology, The University of Tokyo, Tokyo, Japan
(Tel : +81-3-5841-6927; E-mail: {star, shino}@alab.t.u-tokyo.ac.jp)

Abstract: We introduce a novel sensing device named "three-dimensional capture sheet (3DCS)." The cloth-like sheet measures its own 3D shape with no external equipment. It has many potential applications such as 3D modeling, size and shape measurement, wearable motion capture, tactile sensor, and so on. It consists of a lattice structure inside of the sheet, and each link of the structure has a sensor chip consisting of a triaxial accelerometer and a triaxial magnetometer. The sensor chip measures the gravity and the geomagnetic field to obtain the link posture. After all the link postures are obtained, the whole shape of the sheet is reconstructed by combining them. Additionally, owing to the redundancy of the problem, the estimation error (caused by random noise, a distorted magnetic field, and so on) can be corrected. The feasibility and stability of the estimation algorithm are confirmed through simulations, and the prototype is presented.

Keywords: Sensor network, 3D shape, Flexible sensing device, Gravity, Geomagnetic field.

1. INTRODUCTION

Measuring a 3D shape of cloth is an interesting issue in the field of engineering because it has various potential applications. For example, the cloth shape wrapping an object roughly represents its shape and size. The garment shape gives an approximation of the wearer's pose and motion. The new type of man-machine interface for 3D modeling or entertainment will be realized, which can be handled with one's both hands or by several people. The surface deformation of a stuffed toy indicates that someone touched it or changed its pose (i.e. tactile or somatic sensation).

We have proposed a novel cloth-like device that measures its own 3D shape by utilizing a large number of minute sensors distributed on it. The device is named "three-dimensional capture sheet (3DCS)." The conventional methods for cloth capture are optical or vision-based [1-4]. However, such methods are weak against occluding situations. In addition, external equipments such as cameras and light sources are required, which can be drawbacks in the applications listed above. Unlike them, the 3DCS does not suffer from the line-of-sight problem and requires no external equipment.

The proposed approach is motivated by the up-to-date technological developments. It is getting easier to embed a large number of down-sized and low-cost sensors in elastic cloth-like materials, due to the recent advances in CMOS-MEMS [5] and the new sensor networking technology [6].

In this paper, we discuss a realization method of the 3DCS. Fig. 1 shows the illustration of the 3DCS. A lattice structure is mounted on the cloth-like sheet. A triaxial accelerometer and a triaxial magnetometer are attached on each link. They measure the gravitational and the geomagnetic vectors. The posture of the link is calculated from the measured data. After the postures of all the links are obtained, the whole shape of the sheet is computed by combining them. In this method, we need to develop only the sheet equipped with the two types of sensors because both of the gravity and the geomagnetic field are available everywhere on the Earth.

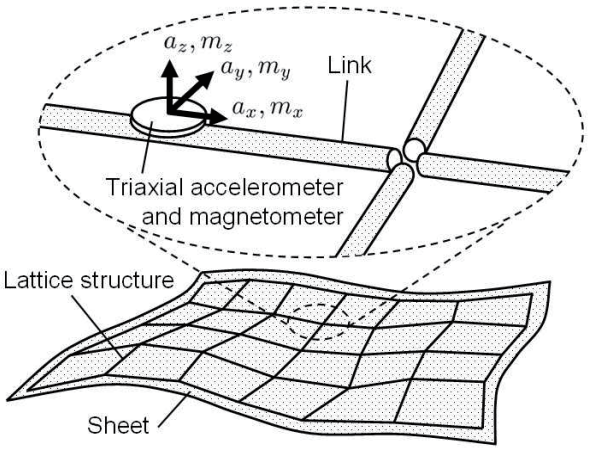

Fig. 1 Illustration of the 3DCS.

In the previous SICE annual conference, we proposed and demonstrated the gravity-based 3DCS [7]. Although it works well in many cases, it has some singular states where reconstruction is impossible. We therefore propose a reinforced method by introducing the Earth's magnetic field as additional information. Gravitational and geomagnetic measurement has been used in motion capture in the preceding reports [8-9]. We apply this technique to the 3DCS.

The following paper outlines, first, a description of the structure and the theory of 3D shape reconstruction. Second, the feasibility of the 3DCS is examined by simulation in Section 3. The prototype is presented in Section 4. Finally, Section 5 concludes this paper.

2. 3D CAPTURE SHEET

2.1 Structure

Fig. 1 shows the illustration of the 3DCS. The 3DCS consists of rigid links forming a lattice structure. A sensor chip is attached on each link which has a triaxial accelerometer and a triaxial magnetometer. The sensors measure the gravitational and the geomagnetic vectors.

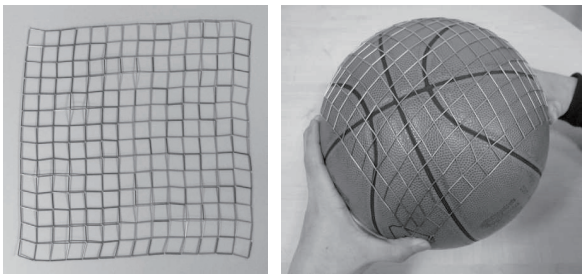

(a) (b)

Fig. 2 (a) 14×14 lattice model made of 1.5 cm rigid tubes combined with strings. (b) The lattice can fit a curved surface.

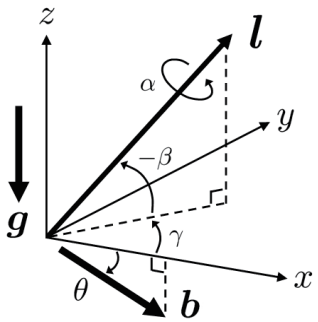

Fig. 3 World coordinate and the posture angles.

The measured data are sent to the host computer. The x-axes of both sensors are aligned to be parallel to the link. The length of each link is the same. The links are connected to each other by free-joints.

Fig. 2 (a) shows the mock-up of the 3DCS consisting of rigid tubes combined with strings. Since the link length does not change, the lattice structure expands or contracts along the diagonal directions, as is the case with a textile cloth. This lattice structure hence can be mounted on the cloth without inhibiting the cloth deformation. As shown in Fig. 2 (b), the structure is able to cover a smooth curved surface.

2.2 Problem settings

First, we introduce the following assumptions to restrict the problem to a static and ideal case.

- Acceleration caused by the link motion is negligible compared with the gravity acceleration.
- There is no considerable magnetic field except for the Earth's magnetic field.

The shape estimation in a dynamic motion or a significantly distorted magnetic field is not considered at least in this stage.

The 3DCS utilizes the gravitational vector **g** and the geomagnetic vector **b** measured with the accelerometer and the magnetometer attached on each link to estimate its configuration. The posture of each link is described by three angles based on the world coordinate (Fig. 3); roll α [rad], pitch β [rad], and yaw γ [rad] ($-\pi \le \alpha < \pi$, $-\pi/2 \le \beta \le \pi/2$, and $0 \le \gamma < 2\pi$). All the angles of each link are calculated from the measured gravitational and geomagnetic data [9], and then the link direction vector **l** is obtained. After all the link direction vectors are obtained, the whole shape of the 3DCS is reconstructed by combining them in a 3D space.

The concrete formulation is as follows. Here we assume that each axis of the sensor is aligned to the corresponding axis of the world coordinate (i.e. the x-axis of the accelerometer to the x-axis of the world coordinate) at the initial condition.

2.3 Derivation of link posture

All the posture angles are derived directly from the gravitational and geomagnetic data measured with the sensor chip on each link. The rotation matrix **G**, from the world coordinate to the sensor coordinate, is described as

$$\mathbf{G} \equiv \begin{bmatrix} c\gamma & -s\gamma & 0 \\ s\gamma & c\gamma & 0 \\ 0 & 0 & 1 \end{bmatrix} \begin{bmatrix} c\beta & 0 & s\beta \\ 0 & 1 & 0 \\ -s\beta & 0 & c\beta \end{bmatrix} \begin{bmatrix} 1 & 0 & 0 \\ 0 & c\alpha & -s\alpha \\ 0 & s\alpha & c\alpha \end{bmatrix} = \begin{bmatrix} c\gamma\, c\beta & c\gamma\, s\beta\, s\alpha - s\gamma\, c\alpha & c\gamma\, s\beta\, c\alpha + s\gamma\, s\alpha \\ s\gamma\, c\beta & s\gamma\, s\beta\, s\alpha + c\gamma\, c\alpha & s\gamma\, s\beta\, c\alpha - c\gamma\, s\alpha \\ -s\beta & c\beta\, s\alpha & c\beta\, c\alpha \end{bmatrix} \quad (1)$$

where "s" and "c" stand for "sin" and "cos", respectively. Each column of **G** means the axis of the sensor coordinate represented in the world coordinate after rotated. The output vector of the accelerometer $\mathbf{a} = [a_x, a_y, a_z]^T$ is represented as a product of the transposed matrix of **G** and the gravitational vector $\mathbf{g} = g\,[0, 0, -1]^T$ (g [m/s^2] is the gravity acceleration);

$$\mathbf{a} = \mathbf{G}^T \mathbf{g} = -g \begin{bmatrix} -s\beta \\ c\beta\, s\alpha \\ c\beta\, c\alpha \end{bmatrix}. \quad (2)$$

Similarly, the output of the magnetometer $\mathbf{m} = [m_x, m_y, m_z]^T$ is represented as a product of $\mathbf{G}^T$ and the geomagnetic vector $\mathbf{b} = b\,[c\theta, 0, -s\theta]^T$ (b [T] is the flux density of the Earth's magnetic field and θ [rad] is the declination angle);

$$\mathbf{m} = \mathbf{G}^T \mathbf{b} = b\,c\theta \begin{bmatrix} c\gamma\, s\beta \\ c\gamma\, s\beta\, s\alpha - s\gamma\, c\alpha \\ c\gamma\, s\beta\, c\alpha + s\gamma\, s\alpha \end{bmatrix} - b\,s\theta \begin{bmatrix} -s\beta \\ c\beta\, s\alpha \\ c\beta\, c\alpha \end{bmatrix}. \quad (3)$$

α, β, and γ are obtained by solving Eqs. (2) and (3) without knowledge of the values of g, b, and θ. For example,

$$\alpha = \tan^{-1}\left(\frac{-a_y}{-a_z}\right), \quad (4)$$

$$\beta = \tan^{-1}\left(\frac{a_x}{\sqrt{a_y^2 + a_z^2}}\right), \quad (5)$$

$$\gamma = \tan^{-1}\left(\frac{-m_y c\alpha + m_z s\alpha}{m_x c\beta + m_y s\alpha\, s\beta + m_z c\alpha\, s\beta}\right). \quad (6)$$

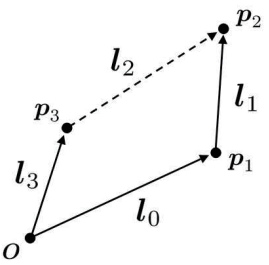

Fig. 4 1×1 lattice structure. The lattice points $\mathbf{p}_1$, $\mathbf{p}_2$, $\mathbf{p}_3$ are represented by only 3 links $\mathbf{l}_0$, $\mathbf{l}_1$, $\mathbf{l}_3$. That means $\mathbf{l}_2$ is redundant.

Eventually, the link direction vector $\mathbf{l}$ is obtained, which consists of β, γ, and the link length l [m];

$$\mathbf{l} \equiv l\mathbf{G}\begin{bmatrix}1\\0\\0\end{bmatrix} = l\begin{bmatrix}\mathrm{c}\gamma\,\mathrm{c}\beta\\ \mathrm{s}\gamma\,\mathrm{c}\beta\\ -\mathrm{s}\beta\end{bmatrix}. \tag{7}$$

After the same algorithm is applied to all the links, the whole configuration is estimated by combining them.

2.4 Redundancy

The reconstruction problem explained above has some redundancy. Here the degree of the redundancy is figured out from the numbers of unknown parameters and available equations. We think about an $N\times N$ lattice structure. N is the number of the links forming one side of the structure. The goal is to determine 3D positions of all the lattice points. While one of the points is fixed as a reference point, the unknown parameters are the three coordinate values for each point; the total number is $3\times\{(N+1)^2-1\}$. On the other hand, the available equations are about the two posture angles (β and γ) and the length (l) for each link; the total number is $3\times 2N(N+1)$. The ratio μ of the parameters to the equations is

$$\mu = \frac{3N(N+2)}{6N(N+1)} \to \frac{1}{2} \quad (N\to\infty)\cdot \tag{8}$$

This means the maximum number of the redundant DOFs is as many as the number of the parameters. The redundancy can be used to reduce effects of noise in a way similar to sensor fusion [10].

For example, we take a case in which $N = 1$. Then μ = 3/4. This is understood as follows. Although the 1×1 lattice structure (lattice unit) is formed by 4 links, the lattice points are determined by only 3 links $\mathbf{l}_0$, $\mathbf{l}_1$, $\mathbf{l}_3$ as shown in Fig. 4. That means the other link $\mathbf{l}_2$ is redundant. $\mathbf{l}_2$ is utilized to elicit an additional vector equation;

$$-\mathbf{l}_3 + \mathbf{l}_0 + \mathbf{l}_1 = \mathbf{l}_2 \cdot \tag{9}$$

By optimizing β_i and γ_i (i is the link identification) according to Eq. (9), they are re-estimated to be more appropriate.

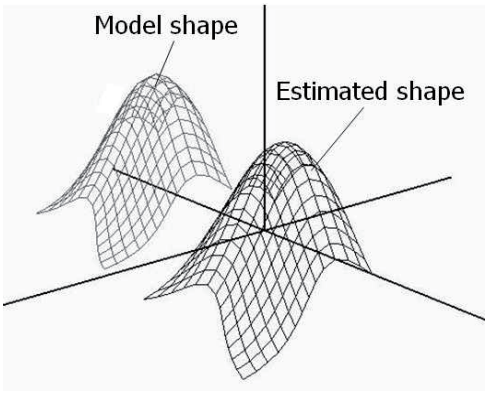

Fig. 5 Simulation results. The far and the near plots are the lattice model and the estimated shape, respectively.

Practically, in order to reduce the number of the parameters in Eq. (9), we fix β_i to the initial value obtained from Eq. (5) and optimize only γ_i. The Earth's magnetic field is easily distorted by magnets, coils, or ferromagnetic materials. That leads to estimation errors on the yaw angles. In contrast, the pitch angles are reliable as long as a static situation keeps since they are derived from the acceleration data.

3. SIMULATIONS AND RESULTS

3.1 Methods

The purpose of the simulation was to confirm if it was feasible to reconstruct the shape of a computational object based on the proposed algorithm. A computational model of a 13×13 lattice structure comprised of links was used as the model of the 3DCS. In this lattice model, the link was modeled as a rigid body so that the link length (2.0 cm) did not change, and the node was modeled as a free-joint.

The lattice model was laid over a target computational shape. The position and posture of each link were determined by iterative calculation of the equation of motion. According to the link posture angles, the outputs of the accelerometer and magnetometer were simulated as the rotated vectors of the virtual gravitational and geomagnetic vectors.

After that, based on the acquired acceleration and magnetic data, the shape of the computational object was estimated. The posture angles α, β, and γ were analytically determined by Eqs. (4), (5), and (6). In order to re-estimate the yaw angle γ, the following numerical calculation was conducted. First, we modify Eq. (9) into a minimization problem, that is

$$P \equiv \sum_{j\in\{x,y,z\}} (l_{0j} + l_{1j} - l_{2j} - l_{3j})^2 \to \min. \tag{10}$$

where j is the coordinate identification. Here, γ_i are unknown parameters. If the minimum value of P is equal to zero, the solutions for Eq. (10) are also the solutions for Eq. (9). Second, we solve Eq. (10) by the conjugate gradient method [11]. The values of γ_i obtained from Eq. (6) are used as the initial values. Accordingly, the probable values of γ_i are obtained.

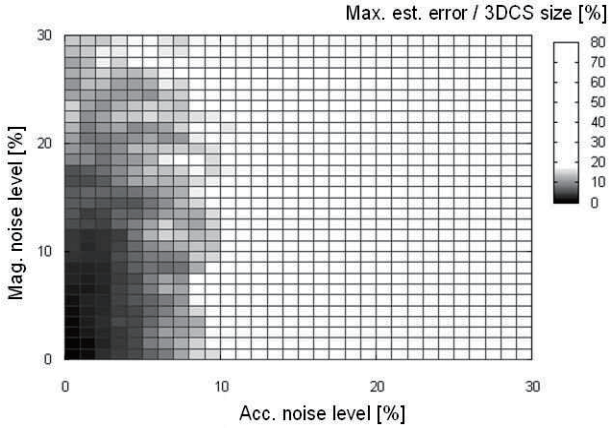

Fig. 6 Simulation results on effects of noise. The worst cases, i.e. the envelope of the error plot, are shown (10 trials per each noise level). The area of the maximum estimation error under 15 % is colored deeply.

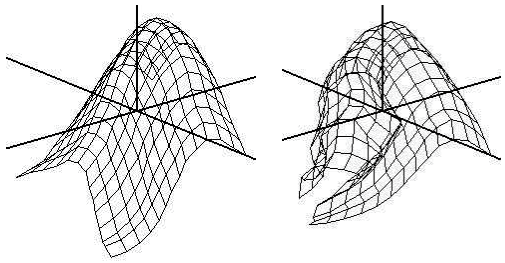

(a) (b)

Fig. 7 Examples in the cases of (a) 5 % acc. and 20 % mag. noises, and (b) 10 % acc. and 20 % mag. noises.

3.2 Results on shape estimation

An example is shown in which a Gaussian is used as a target shape. Fig. 5 shows the computed lattice model laid over the Gaussian shape (plots at far side) and the shape reconstructed from the acceleration and magnetic data (plots at near side). The Gaussian shape is successfully reproduced.

3.3 Effects of acceleration and magnetic noises

The results in Fig. 5 were obtained without considering effects of noise. There are several possible causes of disturbance in the real situation, including random noise on the sensor data, change of the link length, acceleration of motion, and magnetic distortion. Among the causes listed above, the most major cause is considered to be the noise on the sensor data. In order to investigate the stability of the 3DCS under various S/N ratios, the following simulation was carried out.

The simulation was conducted in the same manner as described in Section 3.1, except that noises were added to each component of the acceleration and magnetic data. The noises were generated using the Mersenne Twister algorithm [12]. The acceleration and magnetic noise levels were represented as the percentages compared to the gravity g and the horizontal geomagnetic flux density $b\cos\theta$, respectively.

Fig. 6 shows the maximum values of the estimation errors as the function of the acceleration and magnetic noise levels. The estimation error of each trial is the maximum distance between the corresponding nodes of the lattice model and the reconstructed model, which is normalized by the side length of the 3DCS. The reconstructed shape has uncertainty in the absolute position and posture. Therefore, the estimation error was determined as follows. The sum of the distance between the corresponding nodes of the lattice model and the reconstructed model (i.e. the estimation error sum) was calculated. The absolute position and posture of the reconstructed model were varied so that the estimation error sum was minimized based on the least-square method. Note that if no errors were added to the acceleration and magnetic outputs, the lattice model and the reconstructed shape should be identical. 10 trials per each noise level were conducted. The maximum value of the estimation error among all the nodes was chosen and shown in Fig. 6 for each noise condition.

From our observation of this simulation, it turned out that the maximum estimation error higher than 15 % (i.e. 39 mm) is critical. Based on that benchmark, it was determined that the noise levels were allowed up to 8 % for the acceleration data (i.e. about 0.8 m/s^2) and 25 % for the magnetic data (i.e. about 7.5 μT in Tokyo). Typical examples are shown in Fig. 7; (a) successful and (b) unsuccessful.

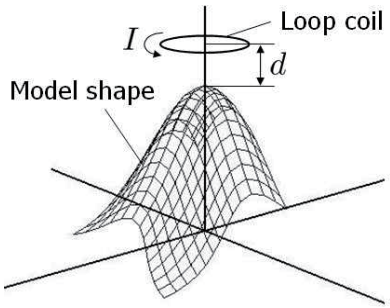

Fig. 8 Simulation setting with a single-loop coil. The diameter is 10 cm and the current I is 10 A.

3.4 Effectiveness of correction algorithm

In order to examine the effectiveness of the correction algorithm described in Section 2.4, the following simulation was carried out. It was conducted in the same manner as described in Section 3.1, except that a single-loop coil (a magnetic source) added an additional magnetic field to the Earth's magnetic field. The coil was parallel to the x-y plane and located just above the model shape at a distance d [m] from the surface of the 3DCS (Fig. 8). The diameter of the coil was 10 cm and the current I [A] was 10 A. The magnetic field arisen from the coil was calculated based on the Biot-Savart law.

Fig. 9 shows the estimation errors as the function of the distances between the top of the model shape and the coil. The distance d is normalized by the link length l. (Here, l = 2.0 cm.) Because this simulation was without random noises, 1 trial per each distance was conducted.

From the results of the simulation, it turned out that the shape was successfully reconstructed even when the coil was located at a distance of 1.8 cm (d/l = 0.9) from

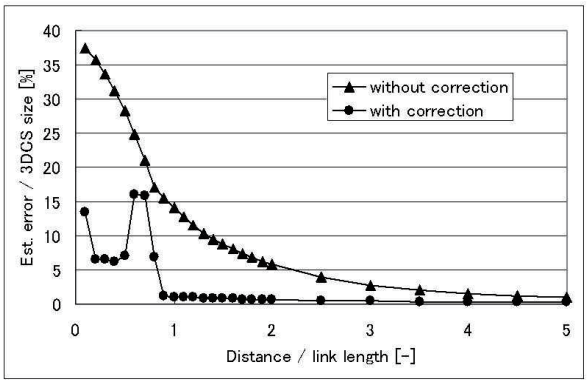

Fig. 9 Simulation results on effectiveness of the correction algorithm. The horizontal axis is the distance d, normalized by the link length l, between the coil and the 3DCS.

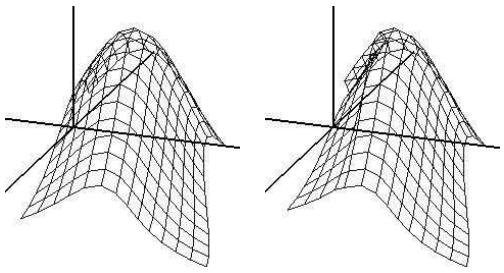

(a) (b)

Fig. 10 Examples in the cases with correction. (a) d/l = 0.9 (error = 1.1 %) and (b) d/l = 0.8 (error = 6.9 %).

the surface of the 3DCS, and the estimation error was as small as 1.1 % (i.e. about 2.9 mm). The same error occurred when d = 9 cm (d/l = 4.5) in the case without correction. That suggests that the estimation algorithm works well unless magnetic sources or ferromagnetic materials come very close to or contact the 3DCS. Typical examples are shown in Fig. 10; (a) successful and (b) unsuccessful.

4. PROTOTYPE

4.1 System specifications

A sensor chip (Fig. 11) was fabricated which has a 6-axis motion sensor (AMI601, 5.2×6.0 mm^2, Aichi Micro Intelligent Corp.). This sensor functions as both a 3-axis accelerometer and a 3-axis magnetometer. The chip also has a microcomputer (PIC18F45J10-I/ML, 8.0×8.0 mm^2, Microchip Technology Inc.) which receives the measured data from the motion sensor and transmits the data to the host PC via an I^{2}C bas line. The operating frequency is 20 MHz. The size of the sensor chip is 13×33 mm^2.

Fig. 12 shows the prototype of the 3DCS. The side length of the lattice structure is 16.5 cm. 24 sensor chips are connected with parallel wires and form a 3×3 lattice structure. At this stage, it is not attached to a piece of cloth. The update rate is now 7 Hz. The optimization of communication and processing is needed for a faster update rate.

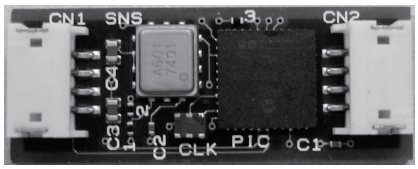

Fig. 11 Fabricated sensor chip (13×33 mm^2). The main components are the 6-axis sensor (SNS, 5.2×6.0 mm^2) and the microcomputer (PIC, 8.0×8.0 mm^2).

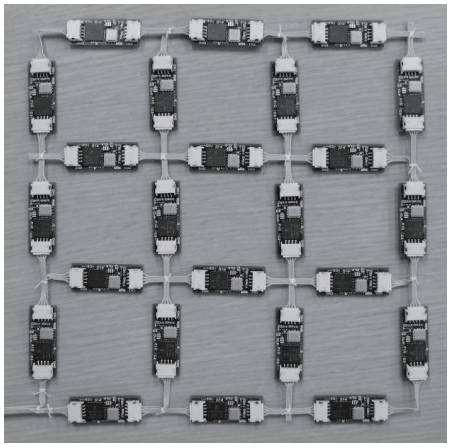

Fig. 12 Prototype of the 3DCS (16.5×16.5 cm^2). 24 sensor chips are used. The sensor chips are connected with parallel wires.

4.2 Demonstration 1: Flat plate

Fig. 13 shows the shape estimation of a flat plate. The 3×3 lattice structure was successfully reconstructed in approximately real-time.

An accuracy evaluation experiment was conducted. The estimated positions of the lattice points were recorded in changing the slope angle of the plate from 0 deg to 90 deg. The slope error was less than 9 deg (6 deg on average) and the position error of the lattice points was less than 15 mm (10 mm on average). These errors were caused by the alignment error and the offset drift of the sensors, the turning characteristics of the wires, and the computational error.

4.3 Demonstration 2: Sphere

Fig. 14 shows the shape estimation of a sphere (23.2 cm in diameter). The lattice structure was also estimated successfully in this case.

5. CONCLUSION

This paper proposed a new flexible sensing device "3DCS," which measures its own 3D configuration utilizing distributed triaxial accelerometers and triaxial magnetometers. The structure and the shape estimation algorithm were described. The feasibility of the algorithm was verified by simulation. The developed prototype was presented.

In the future, we will develop a small-sized sensor chip on which a customized LSI is mounted with a triaxial accelerometer and a triaxial magnetometer. The

LSI is designed to receive the sensor readouts and send digital data to the host computer via the two-dimensional communication sheet [6]. The required electrical power is also supplied via the same sheet to the sensor chips. By installing such advanced technologies, the practical 3DCS will be realized without complicated long signal/power wires.

ACKNOWLEDGMENT

This work is partly supported by JSPS Research Fellowships for Young Scientists.

REFERENCES

[1] P. Fong and F. Buron, "High-resolution three-dimensional sensing of fast deforming objects," *Proc. IEEE/RSJ International Conference on Intelligent Robots and Systems (IROS 2005)*, pp. 1606-1611, 2005.
[2] T. Weise, B. Leibe, and L. V. Gool, "Fast 3D scanning with automatic motion compensation," *Proc. IEEE Conference on Computer Vision and Pattern Recognition (CVPR'07)*, pp. 1-8, 2007.
[3] D. Pritchard and W. Heidrich, "Cloth motion capture," *Proc. EUROGRAPHICS 2003*, vol. 22, pp. 263-271, 2003.
[4] R. White, A. Lobay, and D. Forsyth, "Cloth capture," *UC Berkeley Technical Report*, no. UCB/CSD-5-1387, 2005.
[5] O. Brand, "Microsensor integration into systems-on-chip," *Proc. IEEE*, vol. 94, no. 6, pp. 1160-1176, 2006.
[6] Y. Makino, H. Chigusa and H. Shinoda, "Two-dimensional sensor integration using resonant proximity connector -Basic technology and application to elastic interface device-," *Proc. 3rd International Conference on Networked Sensing Systems (INSS 2006)*, pp. 196-202, 2006.
[7] T. Hoshi and H. Shinoda, "Gravity-based 3D shape measuring sheet," *Proc. SICE Annual Conference 2007*, pp. 2126-2131, 2007.
[8] J. Lee and I. Ha, "Real-time motion capture for a human body using accelerometers," *Robotica*, vol. 19, pp. 601-610, 2001.
[9] D. Fontaine, D. David, Y. Caritu, "Sourceless human body motion capture," *Proc. Smart Objects Conference (SOC'03)*, 2003.
[10] Y. Nakamura and Y. Xu, "Geometrical fusion method for multi-sensor robotic systems," *Proc. 1989 IEEE International Conference on Robotics and Automation (ICRA'89)*, pp. 668-673, 1989.
[11] W. H. Press, S. A. Teukolsky, W. T. Vetterling, and B. P. Flannery, *Numerical Recipes in C: The Art of Scientific Computing Second Edition*, Cambridge University Press, 1992.
[12] M. Matsumoto and T. Nishimura, "Mersenne Twister: A 623-dimensionally equidistributed uniform pseudorandom number generator," *ACM Trans. Modeling and Computer Simulation*, vol. 8, no. 1, pp.3-30, 1998.

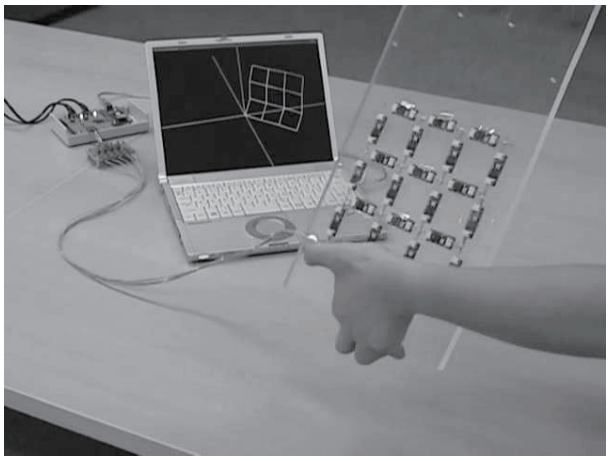

Fig. 13 Demonstration 1: Flat plate.

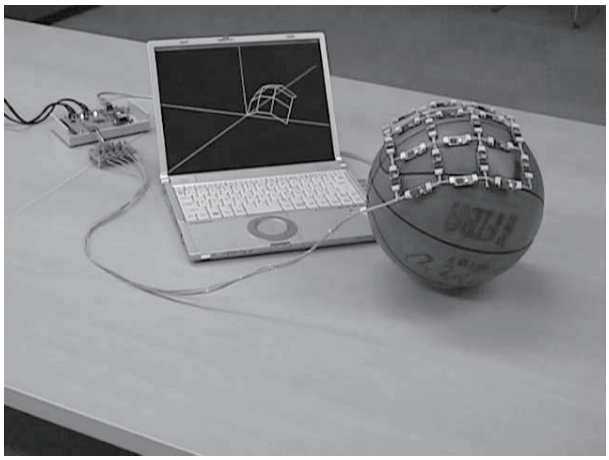

Fig. 14 Demonstration 2: Sphere.